Research Article

Received: 11 January 2025 Revised: 31 January 2025 Published online in Wiley Online Library: 3 March 2025

(wileyonlinelibrary.com) DOI 10.1002/pi.6753

Catalyst-free synthesis, characterization and photoluminescence of main-chain luminescent polybenzoxazines

Kamal I Aly,[a*] Aya Khamies[a] and Osama Younis[b*]

Abstract

Two novel luminescent main-chain polybenzoxazine polymers, $(Poly1)_{main}$ and $(Poly2)^{x}_{main}$, were synthesized and characterized to explore their structural, thermal, morphological and photophysical properties. Polymer $(Poly1)_{main}$ was obtained via a Mannich condensation reaction without a catalyst, followed by thermal polymerization to produce the crosslinked polymer $(Poly2)^{x}_{main}$. Structural analyses using Fourier transform infrared spectroscopy and X-ray diffraction confirmed the successful formation of the polymers, with $(Poly2)^{x}_{main}$ exhibiting a higher degree of crosslinking and partial ordering in an otherwise amorphous structure. Scanning electron microscopy imaging revealed that thermal polymerization significantly altered the morphology, transforming the porous structure of $(Poly1)_{main}$ into a denser, layered morphology in $(Poly2)^{x}_{main}$. Thermogravimetric analysis and differential scanning calorimetry highlighted the improved thermal stability of $(Poly2)^{x}_{main}$ due to extensive crosslinking. Photophysical studies showed that $(Poly1)_{main}$ in solution exhibited yellow-green luminescence with a broad emission maximum at 522 nm and CIE coordinates (0.39, 0.48). In contrast, the powders of both polymers displayed sharp red luminescence with an emission peak at 658 nm and CIE coordinates (0.72, 0.27), attributed to molecular packing effects and exciton coupling in the solid state. These results underscore the interplay among structural, morphological and photophysical properties, highlighting the potential of these polymers in optoelectronics, sensing and luminescent materials.

Keywords: luminescent polymers; main chain; polybenzoxazines; photophysical properties; catalyst-free synthesis

INTRODUCTION

Organic luminescent materials have garnered considerable attention due to their potential applications across a variety of domains, such as organic light-emitting diodes (OLEDs), sensors and bioimaging.[1–8] Small-molecule emitters are known for their well-defined structures and high efficiency; however, they encounter challenges related to stability and thin-film manufacturing.[9–15] In contrast, polymers have emerged as viable luminescent materials.[16–18] They can overcome the limitations associated with small molecules by employing wet processing techniques and having solid-state emissions. Polymeric light-emitting diodes provide the ability to fine-tune the emitted light wavelength and characteristics through adjustments to the polymer chain structure via methods like blending, doping or the addition of spacers.[19,20] The field of luminescent polymers has attracted significant research interest, particularly in the creation of advanced materials such as hyper-crosslinked polymers, porous and π-conjugated polymers, and metal–organic frameworks.[21–31] The capacity to modify optoelectronic properties, the incorporation of fluorescent probes into polymer matrices and the growing need for reusable heterogeneous sensors have all spurred progress in areas such as organic light-emitting polymers, phototherapy and chemical sensing.[32–42] Notably, polymers exhibit excellent film-forming capabilities, allowing for the production of flexible thin films through standard compression-molding techniques.[43–45] Despite their advantages, these polymers frequently face issues with lower emission efficiency due to challenges in polymer chemistry and the presence of defects.[46] Furthermore, difficulties such as limited solvent permeability, poor hydrolytic stability and high densities emphasize the necessity for the development of efficient and stable luminescent materials that maintain their photophysical properties and functionality.[47] Moreover, polymerization products are often contaminated with impurities, including catalyst residues that are difficult to remove through distillation or sublimation. These impurities can trap charge carriers, reducing device efficiency and shortening operational lifespan.[48] As a result, luminescent polymers synthesized without catalysts are highly desirable.

Luminescent polybenzoxazines exhibit light-emitting properties. These polymers are engineered by integrating luminescent components into their framework, making them suitable for applications in sensors, optoelectronics and bioimaging.[49–51] The combination of the favorable attributes of benzoxazine

* *Correspondence to: KI Aly, Polymer Research Laboratory, Chemistry Department, Faculty of Science, Assiut University, Asyut 71516, Egypt, E-mail: kamalaly@aun.edu.eg; or O Younis, Chemistry Department, Faculty of Science, New Valley University, El-Kharga 72511, Egypt, E-mail: osamayounis@sci.nvu.edu.eg*

a *Polymer Research Laboratory, Chemistry Department, Faculty of Science, Assiut University, Asyut, Egypt*

b *Chemistry Department, Faculty of Science, New Valley University, El-Kharga, Egypt*

polymers with light-emitting capabilities renders luminescent polybenzoxazines versatile for diverse applications requiring both thermosetting characteristics and luminescence.[52,53] Benzoxazine is characterized by a heterocyclic six-membered ring containing oxygen and nitrogen atoms. The production of benzoxazines involves dehydrating phenolic compounds, amines and formaldehyde, ending in the formation of polybenzoxazines through thermal ring-opening polymerization.[21–28] The resulting polymer networks comprise crosslinked structures of phenolic units connected by Mannich bridges (—CH_2—NR—CH_2—).[54,55] The stability of these networks is further enhanced by hydrogen bonding, both inter- and intramolecularly. Specifically, the phenolic hydroxyl groups engage in hydrogen bonding with aromatic rings and with oxygen or nitrogen atoms, contributing to high thermal stability and mechanical strength.[56–59] Main-chain polymers are pivotal in luminescence, particularly in the fabrication of advanced materials for optoelectronic devices such as OLEDs, light-emitting electrochemical cells and fluorescent sensors.[48,60,61] Their significance arises from several factors, including substantial structural rigidification, which can enhance emission quantum yield and enable room temperature phosphorescence by reducing free volume compared to side-chain polymers. Additional benefits of main-chain polymers include improved photostability, processability, energy transfer efficiency and environmental stability, facilitating applications in optoelectronics, data storage and security.

In the study reported here, we synthesized two novel luminescent main-chain polybenzoxazine polymers, designated $(Poly1)_{main}$ and $(Poly2)^{x}_{main}$. Polymer $(Poly2)^{x}_{main}$ features a cyclopentanone component and was synthesized through the thermal ring-opening polymerization of $(Poly1)_{main}$ without using a catalyst. A range of comprehensive characterization techniques were employed to evaluate the structure and properties of the polymers, and their luminescent behavior was thoroughly investigated.

EXPERIMENTAL

Materials

Cyclopentanone (99%), methyl alcohol (99.5%), 4,4′-diaminodiphenylmethane (99%), hydrochloric acid (37%), 1,4-dioxane (99.5%), vanillin (100%), paraformaldehyde and ethyl acetate (99%) were purchased from Aldrich (Hamburg, Germany) and used as supplied.

Synthesis of polymers $(Poly1)_{main}$ and $(Poly2)^{x}_{main}$

Synthesis of polymer $(Poly1)_{main}$

A mixture of paraformaldehyde (0.17 g, 5.6 mmol) and 4,4′-diaminodiphenylmethane (0.56 g, 2.8 mmol) was prepared in 40 mL of 1,4-dioxane. This mixture was heated under reflux in a 100 mL round-bottom flask with continuous stirring at 70 °C for 30 min. Following this initial heating, bis-OHOMe (1.00 g, 2.8 mmol) was added, and the temperature gradually increased to 110 °C while stirring for 24 h. During the reaction, precipitation was observed. Upon completion, the mixture was filtered to separate the resulting yellowish residue. To purify this residue, it was suspended in ethyl acetate (EtOAc) with stirring for 2 h, followed by another filtration. The final product obtained was yellow powder and achieved a conversion of 90%. FTIR (KBr, cm^{-1}): 2965 and 2916 (C—H stretching), 1681 (C═O), 1254 (C—O—C, C—N—C asymmetric stretching), 1117 (C—O—C, C—N—C symmetric stretching), 928 (benzoxazine-related mode).

Synthesis of polymer $(Poly2)^{x}_{main}$

Polymer $(Poly2)^{x}_{main}$ was synthesized through the thermal curing polymerization of $(Poly1)_{main}$, as illustrated in Scheme 1. Equal amounts of $(Poly1)_{main}$ were subjected to separate curing treatments at temperatures of 110, 150, 180, 210 and 250 °C, each step lasting 2 h. FTIR (KBr, cm^{-1}): 3430 (OH stretching), 1683 (C═O), 1599 (C═C).

Instrumentation

Fourier transform infrared (FTIR) spectra were obtained with a Shimadzu IR 470 spectrophotometer, utilizing KBr as the matrix, and the maximum wavenumbers were measured in cm^{-1}. For XRD, a scan-type experiment was conducted in fast mode (2θ) using a PSD (1D model) detector, SSD160. To evaluate the thermal stability of the samples, TGA was carried out with a PerkinElmer TGA 4000 instrument. Samples weighing between 5 and 10 mg were placed in alumina crucibles and heated in a nitrogen atmosphere at a rate of 30 °C min^{-1}, covering a temperature range from 50 to 700 °C with a nitrogen flow rate of 20 mL min^{-1}. DSC was performed using a TA Instruments model DSC 2010, with a heating rate of 20 °C min^{-1}. The DSC experiments were conducted in a nitrogen atmosphere to ensure uniform heat distribution within the sample chamber, benefiting from nitrogen's superior heat conductivity. SEM analysis was conducted using a Jeol JSM-5400 LV. Additionally, spectral measurements were performed with a UV spectrophotometer equipped with matched 1.0 cm cells, Vision Pro software from Thermo Electron Corporation (Cambridge, UK) and an Agilent Cary Eclipse fluorescence spectrophotometer.

RESULTS AND DISCUSSION

Synthesis and characterization

This section outlines the synthesis and characterization processes for the main-chain benzoxazine-based polymers, $(Poly1)_{main}$ and $(Poly2)^{x}_{main}$. The synthesis of $(Poly2)^{x}_{main}$ was achieved through a three-step procedure, as shown in Scheme 1. Initially, cyclopentanone was reacted with vanillin, following established methods in the literature, which resulted in the formation of the reported bis-OHOMe.[44,45,62] The second step involved a Mannich condensation reaction, where bis-OHOMe was combined with 4,4′-diaminodiphenylmethane (4,4′-methylenedianiline) in the presence of paraformaldehyde and 1,4-dioxane. This step, which did not require a catalyst, facilitated the ring-closing reaction and led to the synthesis of polymer $(Poly1)_{main}$. In the final stage, $(Poly1)_{main}$ underwent thermal polymerization at 210 °C, yielding the crosslinked polymer $(Poly2)^{x}_{main}$, characterized as a dark brown powder. Table 1 provides a summary of the physical properties of both $(Poly1)_{main}$ and $(Poly2)^{x}_{main}$.

The FTIR spectra of bis-OHOMe, $(Poly1)_{main}$ and $(Poly2)^{x}_{main}$ are illustrated in Fig. 1(a). The FTIR spectrum of bis-OHOMe exhibits distinct absorption bands at 3416 cm^{-1} for the phenolic hydroxyl group, 1673 cm^{-1} for the C═O stretch and 1690 cm^{-1} for the C═C stretching. In the spectrum of $(Poly1)_{main}$, absorption peaks are observed at 2965 and 2916 cm^{-1}, corresponding to C—H stretching in the cyclopentanone unit, a band at 1681 cm^{-1} for the C═O group and bands at 1254 and 1117 cm^{-1} representing asymmetric and symmetric C—O—C stretching, respectively. Additionally, an absorption at 928 cm^{-1} corresponds to the oxazine ring. Upon thermal ring-opening polymerization of $(Poly1)_{main}$ at 210 °C for 2 h, the characteristic bands attributed to the oxazine rings in $(Poly1)_{main}$ disappear, signaling the completion of the

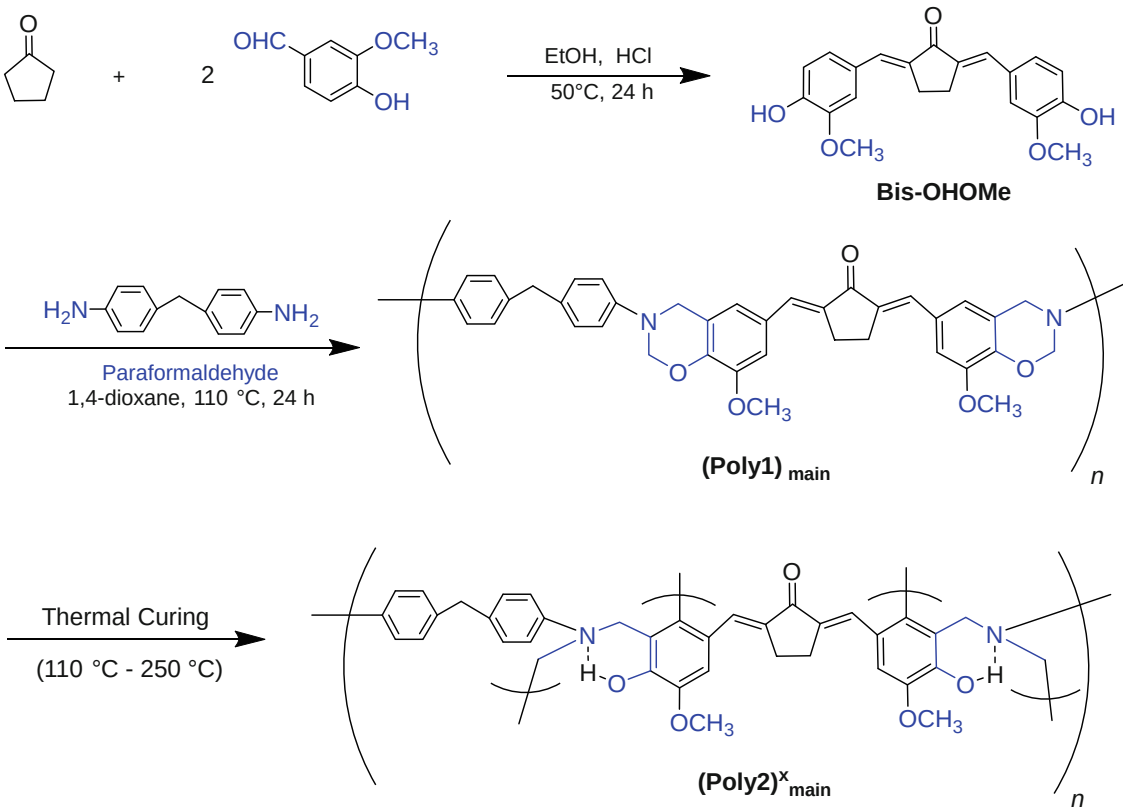

Scheme 1. Synthesis of main-chain benzoxazine-based polymers $(Poly1)_{main}$ and $(Poly2)^{x}_{main}$.

Table 1. Physical properties of $(Poly1)_{main}$ and $(Poly2)^{x}_{main}$

Physical characteristic	$(Poly1)_{main}$	$(Poly2)^{x}_{main}$
State	Solid	Solid
Color	Yellow	Dark brown
Solubility	Partially soluble in DMSO	Insoluble in all organic solvents

ring-opening polymerization and the formation of $(Poly2)^{x}_{main}$. This thermal polymerization was monitored by FTIR spectroscopy (Fig. 1(a),(b)). The absorption bands at 1117 cm^{-1} (symmetric C—O—C stretching) and 1254 cm^{-1} (asymmetric C—O—C stretching) in the FTIR spectrum of $(Poly1)_{main}$ gradually diminish in intensity as the temperature increases from room temperature to 210 °C. The ring-opening polymerization was confirmed to be complete after thermal treatment at 210 °C. Concurrently, a broad absorption band associated with OH groups increases in intensity around 3416 cm^{-1}, further indicating the ring opening of the benzoxazine units. These observations are consistent with the DSC results (Fig. 2(a)), confirming that the oxazine rings in $(Poly1)_{main}$ undergo catalyst-free thermal ring opening to form the highly crosslinked main-chain benzoxazine polymer $(Poly2)^{x}_{main}$.

Thermal behavior

DSC was employed to examine the thermal polymerization process that leads to the crosslinking of $(Poly1)_{main}$, resulting in the formation of $(Poly2)^{x}_{main}$. The DSC thermograms (Fig. 2(a)) illustrate the changes in heat flow for $(Poly1)_{main}$ before and after thermal curing at temperatures of 110, 150, 180, 210 and 250 °C. These graphs highlight the temperature-dependent reaction, revealing how heat flow varies with increasing temperature. For the uncured samples and those cured at 110, 150 and 180 °C, the heat flow remains relatively low at lower temperatures, indicating that $(Poly1)_{main}$ is stable in its initial state. As the temperature increases to around 200 °C, a significant rise in heat flow is observed, signaling the onset of the ring-opening polymerization process. The curves on the graph reflect the reaction progression as the temperature continues to climb, showing an upward trend that corresponds to the transition of $(Poly1)_{main}$ from its initial state to a higher energy state. This transition is linked to the ring opening of the oxazine in $(Poly1)_{main}$ and the subsequent formation of $(Poly2)^{x}_{main}$. For the samples cured at 210 and 250 °C, the heat flow remains relatively constant even at high temperatures, indicating the complete formation of $(Poly2)^{x}_{main}$ in those two samples. These DSC results suggest that higher temperatures (210 and 250 °C) accelerate the reaction rate of the ring-opening polymerization of the oxazine $(Poly1)_{main}$. Thermal treatments at 110, 150 and 180 °C display progressively increased reaction rates, indicating favorable conditions for polymerization. However, at 210 °C, the reaction rate reaches maximum, suggesting that higher temperatures may not be as efficient, whereas the analysis does not indicate any advantage for thermal curing at 250 °C.

The thermal behavior of $(Poly1)_{main}$ and $(Poly2)^{x}_{main}$ was examined before and after curing at various temperatures (110, 150, 180, 210 and 250 °C) using TGA, as shown in Fig. 2(b). TGA revealed that the uncured $(Poly1)_{main}$ displayed significant weight loss at low temperatures, indicating its thermal instability and

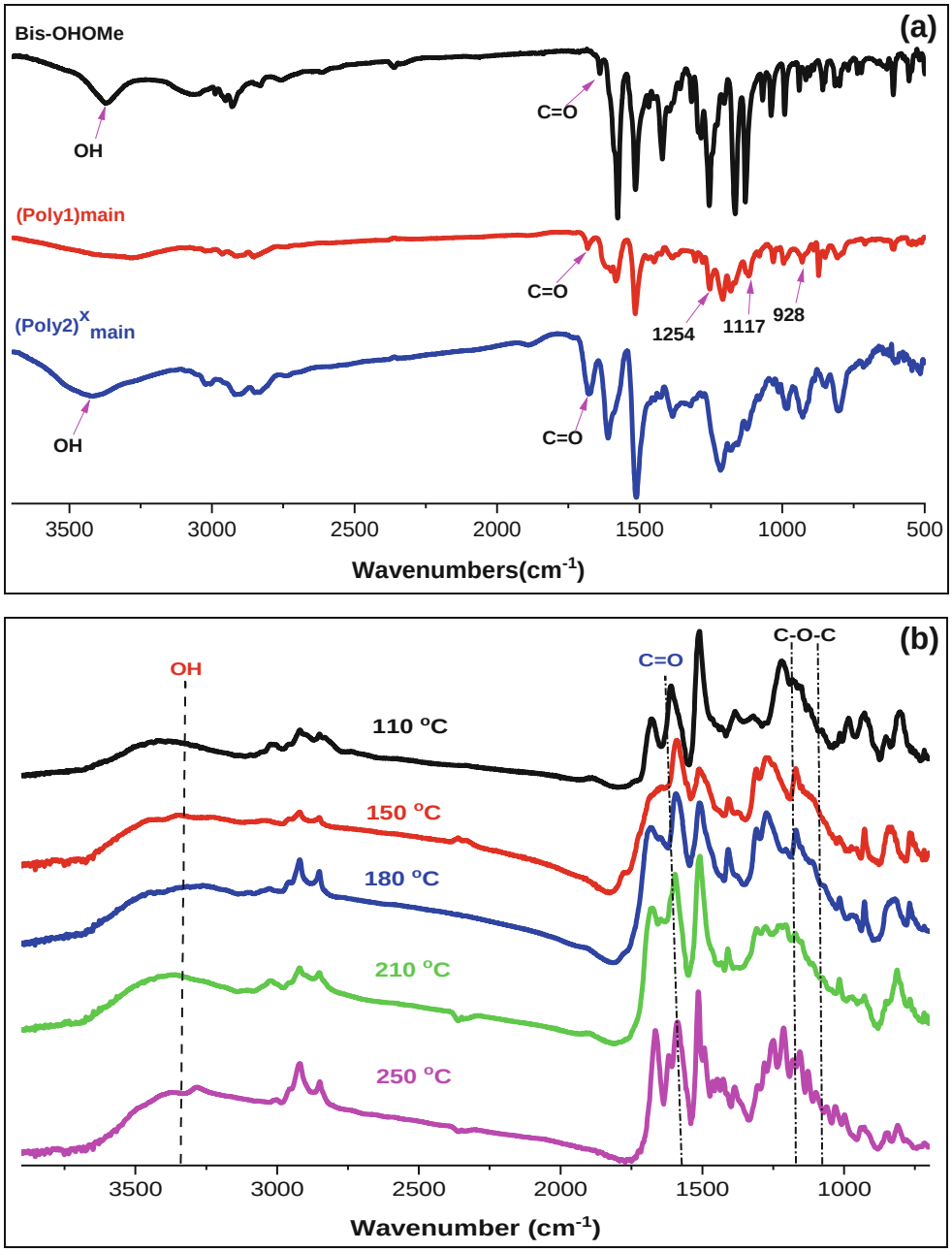

Figure 1. (a) FTIR spectra of bis-OHOMe (black line; adapted with permission from Younis *et al.*[62] Copyright © 2024 John Wiley & Sons Ltd), $(Poly1)_{main}$, and $(Poly2)^{x}_{main}$. (b) FTIR spectra of $(Poly1)_{main}$ to form $(Poly2)^{x}_{main}$ after thermal treatment at different temperatures.

susceptibility to decomposition. However, as the curing temperature increased, the weight loss diminished, suggesting that the resulting polymer, $(Poly2)^{x}_{main}$, achieved greater thermal stability due to crosslinking. This enhanced stability was reflected by the reduced weight loss observed at higher curing temperatures. TGA provided valuable insights into the thermal stability and transformation of $(Poly1)_{main}$ into the more stable $(Poly2)^{x}_{main}$ during the curing process. Crosslinked main-chain polymers like $(Poly2)^{x}_{main}$ demonstrated significantly improved thermal stability compared to polymers derived from monomeric benzoxazine without crosslinking, such as $(Poly1)_{main}$. Thermal stability was characterized by measuring the temperatures at which the samples experienced 5% (T_{d5}) and 10% (T_{d10}) weight loss, as well as the char yield at 700 °C, with results summarized in Table 2. T_{d5} and T_{d10} values were determined from the TGA thermograms by identifying the corresponding temperatures at which the sample mass decreased by 5% and 10%, respectively. The char yield was obtained from the residual weight percentage at 700 °C using the equation: char yield (%) = (mass of char at 700 °C/initial mass of sample) × 100. The char yield reflects the material resistance to thermal decomposition. Higher char yield percentages suggest that the polymer can withstand elevated temperatures without significant degradation, which is a crucial characteristic for applications requiring thermal resistance. The observed increase in T_{d5}, T_{d10} and char yield with higher curing temperatures indicates enhanced crosslinking, leading to improved thermal stability. The high char yield of $(Poly2)^{x}_{main}$ suggests the formation of a robust crosslinked network, which enhances its thermal resistance. These

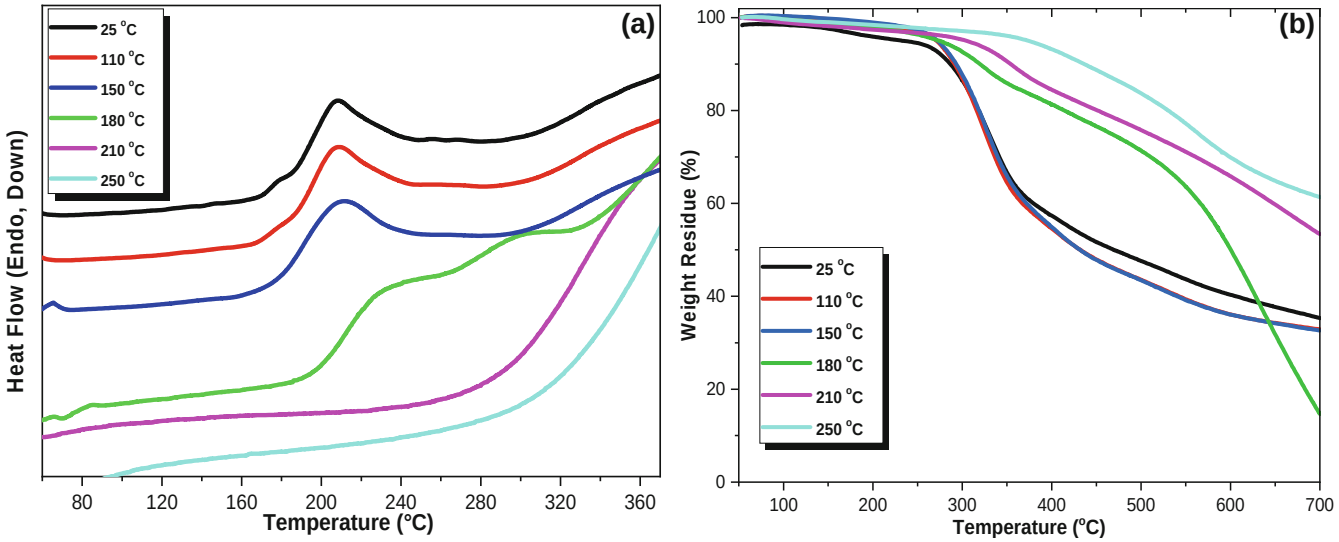

Figure 2. (a) DSC and (b) TGA curves of $(Poly1)_{main}$ under thermal treatment to form $(Poly2)^{x}_{main}$.

Table 2. TGA data for samples cured at different temperatures to transform $(Poly1)_{main}$ into $(Poly2)^{x}_{main}$

Curing temperature (°C)	T_{d5} (°C)	T_{d10} (°C)	Char yield (%)
Uncured	232	292	35
110	274	292	32
150	274	293	32
180	275	319	14
210	304	354	53
250	373	435	61

findings demonstrate that the curing process effectively reinforces the polymer structure, resulting in superior thermal stability compared to its uncured counterpart $(Poly1)_{main}$.

Morphological study

The provided SEM images (Fig. 3) offer insightful visualizations of the structural characteristics of the main-chain benzoxazine-based polymers $(Poly1)_{main}$ and $(Poly2)^{x}_{main}$. In the first set of images (Fig. 3(a)), the SEM micrographs of $(Poly1)_{main}$ at various magnifications reveal a relatively uniform and porous morphology. The polymer exhibits an interconnected network of irregular, globular structures with a rough surface texture. This morphology is likely a result of the Mannich condensation reaction between bis-OHOMe and 4,4′-diaminodiphenylmethane, which led to the formation of $(Poly1)_{main}$. The second set of images (Fig. 3(b)) focuses on the SEM micrographs of $(Poly2)^{x}_{main}$, also captured at different magnifications. These images show a more consolidated and dense morphology compared to $(Poly1)_{main}$. $(Poly2)^{x}_{main}$ polymer exhibits a compact, layered structure with fewer porous features. This distinct morphological change can be attributed to the thermal polymerization of $(Poly1)_{main}$ at 210 °C, which induced the ring opening and crosslinking of the benzoxazine units, resulting in the formation of the highly crosslinked $(Poly2)^{x}_{main}$. The observed structural differences between $(Poly1)_{main}$ and $(Poly2)^{x}_{main}$ provide valuable insights into the impact of the thermal polymerization process on the polymer morphology. The transition from a more porous, irregular structure in $(Poly1)_{main}$ to a denser, layered morphology in $(Poly2)^{x}_{main}$ suggests that the thermal treatment significantly alters the polymer microstructure. These SEM analyses complement the information provided in the earlier sections, which detailed the synthesis of these main-chain benzoxazine-based polymers and the thermal characterization techniques used to study their behavior. The combination of these analytical techniques offers a comprehensive understanding of the structural and morphological changes that occur during the transformation from $(Poly1)_{main}$ to $(Poly2)^{x}_{main}$.

X-ray diffraction

The XRD patterns of the main-chain benzoxazine-based polymers $(Poly1)_{main}$ and $(Poly2)^{x}_{main}$ are shown in Fig. 4. Both polymers exhibit primarily amorphous characteristics, as indicated by the broad, diffuse halo-like features centered around $2\theta = 20°$. However, the presence of a few sharp, well-defined peaks superimposed on the amorphous halos suggests the existence of some minor crystalline regions or ordered domains within the predominantly amorphous polymer structures. For $(Poly1)_{main}$ in Fig. 4(a), the slightly sharp peaks imply the possible presence of little localized areas of short-range order within the overall amorphous matrix. Similarly, the XRD pattern of $(Poly2)^{x}_{main}$ in Fig. 4(b) displays a combination of the broad, amorphous halo and sharper crystalline-like peaks, indicating that the thermal polymerization process did not completely eliminate the amorphous character of the material. Rather, it may have introduced a more complex structural organization, with a mixture of amorphous and partially ordered regions, rather than a clear transition from a fully amorphous to a highly crystalline structure. These observations provide valuable insights into the structural features of these main-chain benzoxazine-based polymers and the impact of the thermal treatment on their overall morphological characteristics.

Absorption, excitation and emission

Due to the insoluble nature of $(Poly2)^{x}_{main}$ in organic solvents, the photophysical properties such as absorption, excitation and emission spectra could not be measured in solution. The insolubility of $(Poly2)^{x}_{main}$ is likely associated with the higher degree of

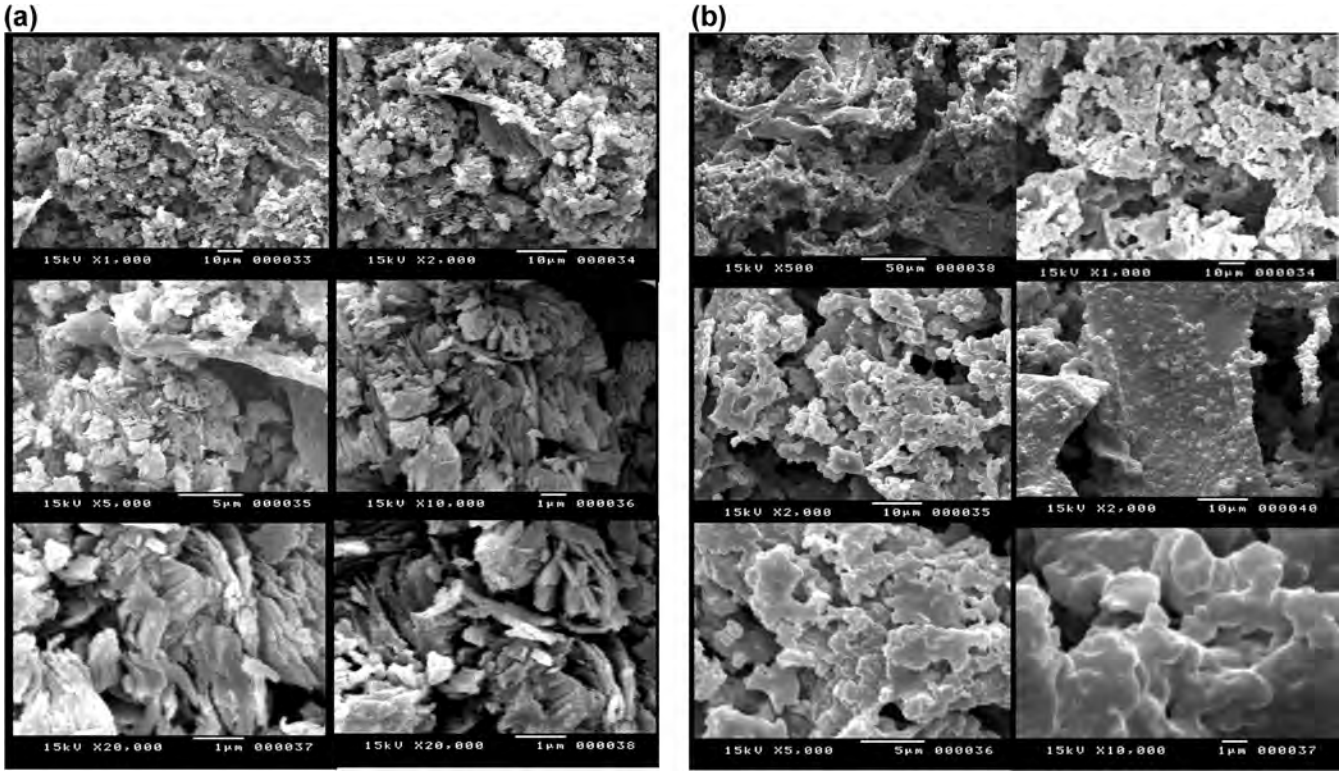

Fig. 3. SEM images of the polymers: (a) $(Poly1)_{main}$; (b) $(Poly2)^{x}_{main}$.

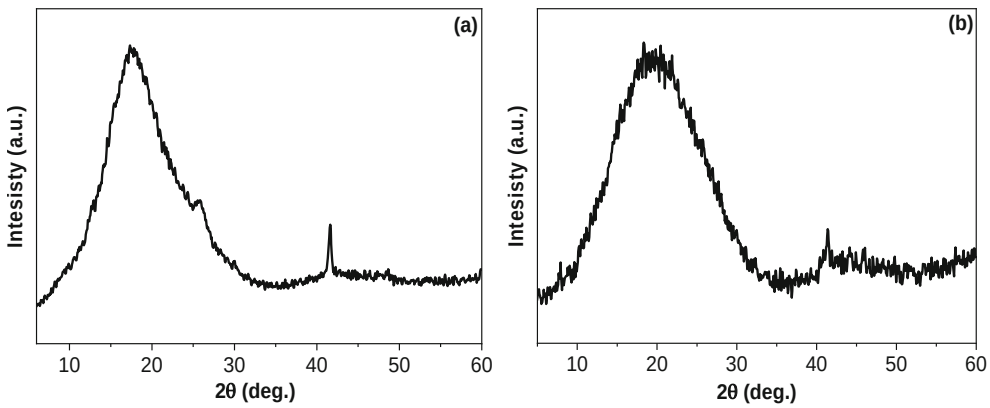

Figure 4. XRD patterns of polymers: (a) $(Poly1)_{main}$; (b) $(Poly2)^{x}_{main}$.

crosslinking and structural changes introduced by the thermal polymerization process. However, $(Poly1)_{main}$ was found to be soluble in DMSO, allowing for the characterization of its solution-phase photophysical behavior, as shown in Fig. 5. The absorption spectrum of $(Poly1)_{main}$ solution exhibits a maximum absorption peak at 400 nm, indicating the electronic transitions associated with the conjugated structure of the polymer that influence the π–π^* transitions (Fig. 5(a)). The absence of significant absorption beyond 500 nm implies that the polymer is transparent in the visible region beyond this point, aligning with its potential applications in optoelectronic devices or as a matrix material. The extinction coefficient of 2×10^4 suggests a moderately strong ability to absorb light at the observed wavelength.

The excitation spectrum provides insights into the wavelengths of light that efficiently promote a polymer from its ground state to an excited state, subsequently leading to fluorescence. For $(Poly1)_{main}$, the maximum excitation at 330 nm, with a minor shoulder at 295 nm, indicates that the polymer can absorb higher-energy UV light and convert it into an emissive state (Fig. 5(b)). The slightly different shape of the excitation spectrum compared to the absorption spectrum highlights that the emitting species might involve a subset of electronic transitions or specific molecular conformations within the polymer. This difference also suggests that the electronic transitions responsible for the absorption and excitation processes are not entirely identical, potentially due to the complex molecular structure and interactions within the polymer.

The emission spectrum of $(Poly1)_{main}$ reveals an interesting photoluminescent behavior (Fig. 5(c)). The polymer shows minimal emission at wavelengths below 450 nm, followed by a

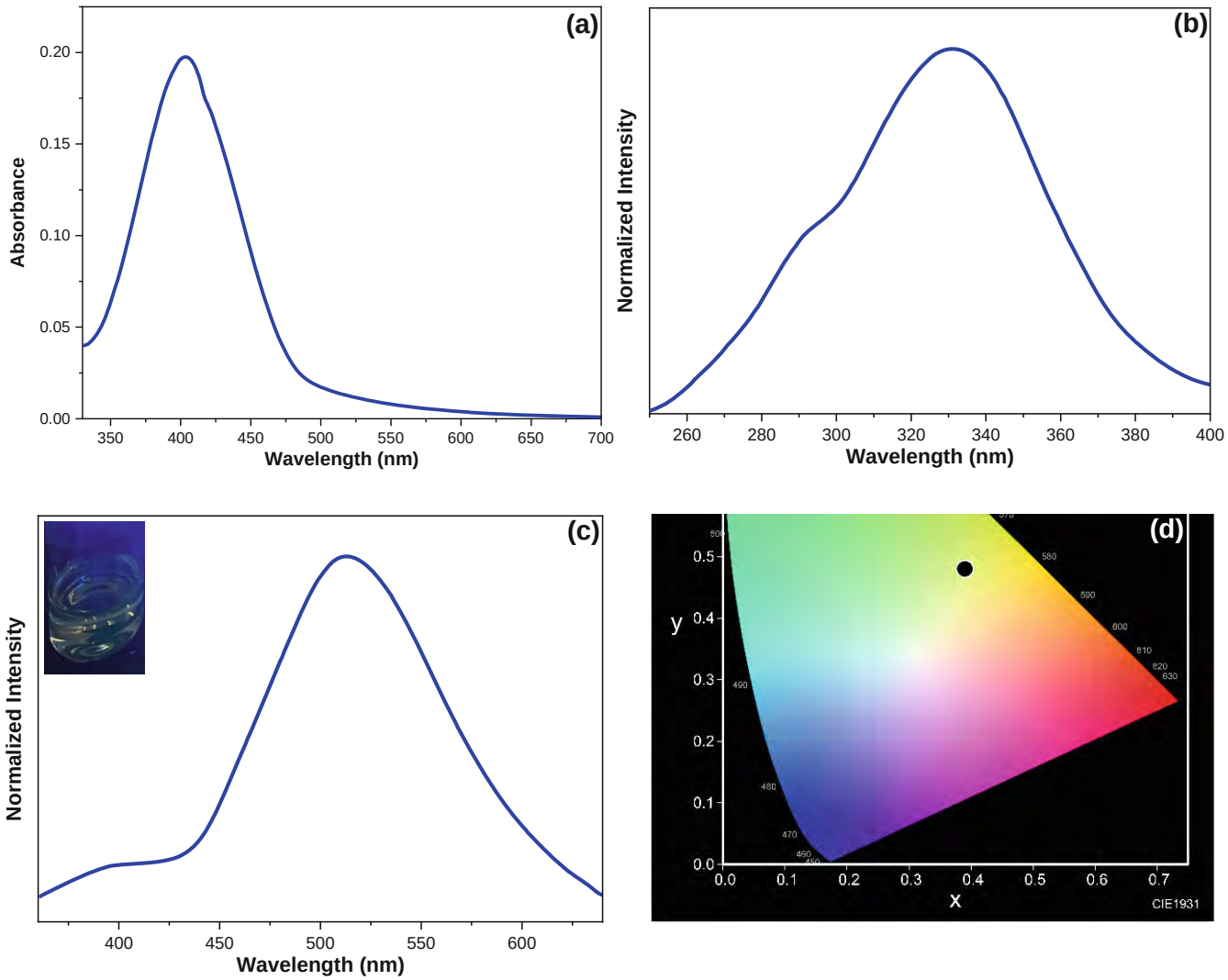

Figure 5. Photophysical properties of $(Poly1)_{main}$ DMSO solution (1×10^{-5} mol L^{-1}): (a) absorption spectrum; (b) excitation spectrum at 522 nm; (c) emission spectrum at 330 nm (inset is a photo under UV illumination at 365 nm); (d) CIE chromaticity diagram.

gradual increase in intensity, reaching a maximum at 522 nm. The emission then decreases in intensity at higher wavelengths, but the polymer remains emissive across a broad spectral range. This broad emission profile suggests a combination of radiative decay processes from excited states, possibly involving multiple electronic transitions or a range of molecular conformations. The Commission Internationale de l'Éclairage (CIE) color coordinates calculated for the $(Poly1)_{main}$ emission spectrum are (0.39, 0.48), indicating a yellowish-green color (Fig. 5(d)). The observed yellow-green color implies that the emitted light is centered around the green part of the visible spectrum, with contributions from yellow. This observation is consistent with the visual appearance of the polymer under UV illumination, as shown in the inset of Fig. 5(c). The photophysical behavior of $(Poly1)_{main}$ likely arises from its aromatic backbone and the presence of functional groups formed during the Mannich condensation step. The interplay among conjugation, inter- or intramolecular interactions and the electronic nature of substituents affects the absorption and emission characteristics. In particular, molecular packing and the polymer structural flexibility in solution influence the transition to the excited state (indicated by the absorption and excitation peaks) and subsequent radiative decay (manifested in the emission spectrum). The combination of the strong light absorption, broad emission spectrum and the resulting yellowish-green color suggest that $(Poly1)_{main}$ may have potential applications in optoelectronic and photonic devices, such as fluorescent probes, light-emitting diodes or luminescent materials.

The photophysical properties of $(Poly1)_{main}$ and $(Poly2)^{x}_{main}$ were further investigated in their powder forms, as shown in Fig. 6. In the powder form, the excitation spectra of both $(Poly1)_{main}$ and $(Poly2)^{x}_{main}$ are identical, with a sharp maximum at 330 nm, indicating that the electronic environment in the solid state is primarily governed by the polymer backbone, with minimal influence from structural differences introduced during thermal polymerization (Fig. 6(a)). The sharp excitation spectrum of the powder polymers indicates a homogeneous and rigid electronic environment. The absence of solvent effects may lead to a uniform electronic excitation. In contrast, the excitation spectrum of $(Poly1)_{main}$ in solution exhibits a broader profile with a maximum at 330 nm and a shoulder at 295 nm, reflecting the influence of solvent interactions and molecular flexibility, which stabilizes certain molecular conformations, leading to slightly

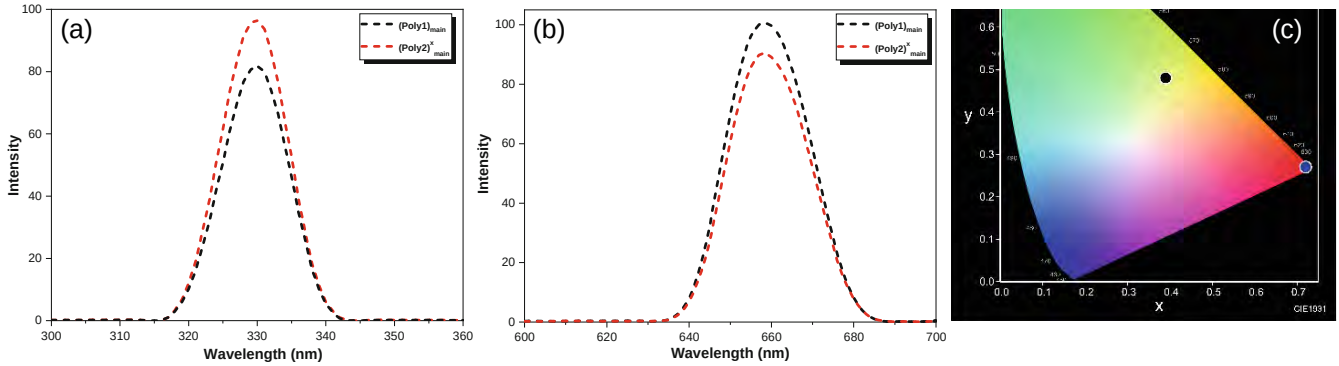

Figure 6. (a) Excitation spectra at 658 nm for powders of $(Poly1)_{main}$ and $(Poly2)^{x}_{main}$. (b) Emission spectra at 330 nm for powders of $(Poly1)_{main}$ and $(Poly2)^{x}_{main}$. (c) CIE chromaticity diagram to compare the emission color from powders of the two polymers (blue circle, both polymers have the same coordinates) and the emission color from the solution of $(Poly1)_{main}$ (black circle).

varied excitation pathways (Fig. 5(b)). Interestingly, the emission spectra of the two polymer powders are also identical, with a sharp, intense peak centered at 658 nm (Fig. 6(b)). This narrow red emission of the powder polymers suggests strong radiative decay from a well-defined excited state, likely influenced by the exciton coupling, rigid molecular packing and restricted motion in the solid state. The observed red shift in the emission spectra of the powder polymers (maximum at 658 nm) compared to solution (maximum at 522 nm; Fig. 6(c)) is common for organic materials. It suggests aggregation effects or π–π stacking interactions that alter the radiative decay pathway, favoring red emission. The red shift also indicates that the emissive properties are influenced by the solid-state packing and intermolecular interactions within the molecular aggregation of the powder samples. The CIE color coordinates calculated for the polymer powders are (0.72, 0.27), corresponding to a deep red color. This red emission is in stark contrast to the yellowish-green color observed for $(Poly1)_{main}$ in solution (CIE coordinates of 0.39, 0.48) (Fig. 6(c)). The differences in the photophysical properties between the polymer solution and powder highlight the significant impact of the solid-state environment on the optical and luminescent characteristics of these main-chain benzoxazine-based materials. The similarities in the excitation and emission spectra of $(Poly1)_{main}$ and $(Poly2)^{x}_{main}$ powders suggest that the thermal polymerization process does not drastically alter the underlying electronic structure and transitions responsible for the photophysical behavior, despite the observed changes in the polymer morphology and solubility.

CONCLUSION

Two luminescent main-chain polybenzoxazine polymers, $(Poly1)_{main}$ and $(Poly2)^{x}_{main}$, were synthesized and extensively characterized to evaluate their structural, thermal, morphological and photophysical properties. The catalyst-free Mannich condensation reaction used to synthesize $(Poly1)_{main}$, followed by thermal polymerization to form $(Poly2)^{x}_{main}$, resulted in polymers with distinct morphologies and photophysical characteristics. XRD analysis revealed that both polymers are primarily amorphous with minor crystalline regions. At the same time, SEM imaging showed a significant transformation from the porous structure of $(Poly1)_{main}$ to the denser, layered morphology of $(Poly2)^{x}_{main}$. Thermal analysis demonstrated the enhanced thermal stability of $(Poly2)^{x}_{main}$, attributed to its high degree of crosslinking. Photophysical investigations highlighted the state-dependent emission behavior of these polymers. In solution, $(Poly1)_{main}$ exhibited yellow-green luminescence (emission maximum at 522 nm), whereas in powder form, both polymers displayed sharp red luminescence (emission maximum at 658 nm), driven by molecular packing and exciton coupling effects. These findings underscore the tunable optical and morphological properties of main-chain polybenzoxazines, offering insights into their potential applications in optoelectronic devices, sensors and luminescent materials. Additionally, the results highlight the importance of catalyst-free synthesis and thermal processing in tailoring the properties of luminescent polymers.

ACKNOWLEDGEMENTS

This work was supported by the Science, Technology & Innovation Funding Authority (STDF) in Egypt as a part of research project ID 49045.

DATA AVAILABILITY STATEMENT

The data provided in this study can be found in the article.

CONFLICT OF INTEREST

The authors declare that they have no competing interests.

AUTHOR CONTRIBUTIONS

Kamal I Aly: Conceptualization, Validation, Visualization, Formal analysis, Investigation, Supervision, Funding acquisition, Project administration, Writing – review & editing. Aya Khamies: Formal analysis, Investigation, Writing – original draft, Writing – review & editing. Osama Younis: Conceptualization, Validation, Visualization, Formal analysis, Investigation, Supervision, Writing – original draft, Writing – review & editing.

REFERENCES

1 Zhu H, Lin CC, Luo W, Shu S, Liu Z, Liu Y *et al.*, *Nat Commun* **5**:4312 (2014).
2 Zhang Q, Li B, Huang S, Nomura H, Tanaka H and Adachi C, *Nat Photon* **8**:326–332 (2014).
3 Yang C, Qi D, Liang J, Wang X, Cao F, He Y *et al.*, *Laser Phys Lett* **15**: 116202 (2018).
4 Grimsdale AC, Leok Chan K, Martin RE, Jokisz PG and Holmes AB, *Chem Rev* **109**:897–1091 (2009).

5 Basabe-Desmonts L, Reinhoudt DN and Crego-Calama M, *Chem Soc Rev* **36**:993–1017 (2007).
6 Sinkeldam RW, Greco NJ and Tor Y, *Chem Rev* **110**:2579–2619 (2010).
7 Younis O, Tolba MS, Orabi EA, Kamal AM, Hassanien R, Tsutsumi O *et al.*, *J Photochem Photobiol A* **400**:112642 (2020).
8 Younis O, Sami H, Maruoka Y, Hisano K and Tsutsumi O, *Dyes Pigm* **194**: 109621 (2021).
9 Jones BA, Facchetti A, Wasielewski MR and Marks TJ, *J Am Chem Soc* **129**:15259–15278 (2007).
10 Zheng Q, Juette MF, Jockusch S, Wasserman MR, Zhou Z, Altman RB *et al.*, *Chem Soc Rev* **43**:1044–1056 (2014).
11 Wu D, Sedgwick AC, Gunnlaugsson T, Akkaya EU, Yoon J and James TD, *Chem Soc Rev* **46**:7105–7123 (2017).
12 Uoyama H, Goushi K, Shizu K, Nomura H and Adachi C, *Nature* **492**: 234–238 (2012).
13 Younis O, Rokusha Y, Sugimoto N, Fujisawa K, Yamada S and Tsutsumi O, *Mol Cryst Liq Cryst* **617**:21–31 (2015).
14 Younis O, El-Katori EE, Hassanien R, Abousalem AS and Tsutsumi O, *Dyes Pigm* **175**:108146 (2020).
15 Younis O, Al-Hossainy AF, Sayed M, Kamal El-dean AM and Tolba MS, *J Photochem Photobiol A* **431**:113992 (2022).
16 Dhbaibi K, Shen C, Jean M, Vanthuyne N, Roisnel T, Górecki M *et al.*, *Front Chem* **8**:237 (2020).
17 Otsuka T and Chujo Y, *J Mater Chem* **20**:10688–10695 (2010).
18 Jia Y, Ma H, Yang J and Ma M, *Polym Int* **72**:1038–1046 (2023).
19 Singha NR, Chattopadhyay PK, Deb M, Karmakar M, Mahapatra M, Mitra M *et al.*, *Luminescent Polymer Light-Emitting Devices and Displays, Polymers for Light-Emitting Devices and Displays*. Scrivener Publishing LLC, Beverly, pp. 125–176 (2020).
20 Wu F, Zhang X, Wang Q, Yu D, Zheng P, Zhu R *et al.*, *Polym Int* **73**:385–392 (2024).
21 Davankov VA and Tsyurupa MP, *React Polym* **13**:27–42 (1990).
22 Xu Y, Chen L, Guo Z, Nagai A and Jiang D, *J Am Chem Soc* **133**:17622–17625 (2011).
23 Budd PM, Ghanem BS, Makhseed S, McKeown NB, Msayib KJ and Tattershall CE, *Chem Commun* **2**:230–231 (2004).
24 Li Y, He Y, Guo F, Zhang S, Liu Y, Lustig WP *et al.*, *ACS Appl Mater Interfaces* **11**:27394–27401 (2019).
25 Chen D, Liu C, Tang J, Luo L and Yu G, *Polym Chem* **10**:1168–1181 (2019).
26 Watanabe K and Akagi K, *Sci Technol Adv Mater* **15**:044203 (2014).
27 Yaghi OM, Li G and Li H, *Nature* **378**:703–706 (1995).
28 Cui Y, Yue Y, Qian G and Chen B, *Chem Rev* **112**:1126–1162 (2012).
29 Younis O, Abdel-Hakim M, Sayed MM, Tsutsumi O and Aly KI, *JOL* **239**: 118361 (2021).
30 Aly KI, Sayed MM, Mohamed MG, Kuo SW and Younis O, *Micropor Mesopor Mater* **298**:110063 (2020).
31 Yang W, Kuai M, Wu C, Yang W, Cao L, Zhang Y *et al.*, *Polym Int* **73**:141–148 (2024).
32 Li Z, Feng X, Gao S, Jin Y, Zhao W, Liu H *et al.*, *ACS Appl Bio Mater* **2**:613–618 (2019).
33 Lu K, He C and Lin W, *J Am Chem Soc* **136**:16712–16715 (2014).
34 Mondal T, Mondal S, Bose S, Sengupta D, Ghorai UK and Saha SK, *J Mater Chem* **6**:614–621 (2018).
35 Lan G, Ni K and Lin W, *Coord Chem Rev* **379**:65–81 (2019).
36 Chen R, Chen W-C, Yan L, Tian S, Liu B, Chen X *et al.*, *J Mater Chem B* **7**: 4763–4770 (2019).
37 Gu C, Chen Y, Zhang Z, Xue S, Sun S, Zhang K *et al.*, *Adv Mater* **25**:3443–3448 (2013).
38 Pallavi P, Bandyopadhyay S, Louis J, Deshmukh A and Patra A, *Chem Commun* **53**:1257–1260 (2017).
39 Bi S, Li Y, Zhang S, Hu J, Wang L and Liu H, *J Mater Chem C* **6**:3961–3967 (2018).
40 Deshmukh A, Bandyopadhyay S, James A and Patra A, *J Mater Chem C* **4**:4427–4433 (2016).
41 Aly KI, Younis O, Mahross MH, Tsutsumi O, Mohamed MG and Sayed MM, *Polym J* **51**:77–90 (2019).
42 Liu P, Deng Y, Lu J, Gou X, Han Q, Pei Y-R *et al.*, *Polym Int* **73**:359–367 (2024).
43 Wang T, Wang J, Liao G, Wang W, Qiu Y, Yin G *et al.*, *Eur Polym J* **199**: 112448 (2023).
44 Abd-Alla MA, Kandeel MM, Aly KI and Hammam AS, *J Macromol Sci A* **27**:523–538 (1990).
45 Abd-Alla MA and Aly KI, *High Perform Polym* **2**:223–234 (1990).
46 Yang S, Streater D, Fiankor C, Zhang J and Huang J, *J Am Chem Soc* **143**: 1061–1068 (2021).
47 Haug WK, Moscarello EM, Wolfson ER and McGrier PL, *Chem Soc Rev* **49**: 839–864 (2020).
48 Cloutet E, Olivero C, Adès D, Castex MC and Siove A, *Polymer* **43**:3489–3495 (2002).
49 Liu H-C, Su W-C and Liu Y-L, *J Mater Chem* **21**:7182–7187 (2011).
50 Goto M, Yajima T, Minami M, Sogawa H and Sanda F, *Macromolecules* **53**:6640–6648 (2020).
51 Saravanamuthu A, Khaja Najimudeen MM, Balaji K, Mani KS, Govindasamy R and Muthukaruppan A, *Polym Int* (2024).
52 Zhu C, Xu H, Geng P and Lu Z, *High Perform Polym* **27**:217–225 (2014).
53 Li W, Yuan X, Huang J, Peng B, Zhou F, Ma J *et al.*, *Polymer* **109**:126–136 (2017).
54 Zhang S, Ran Q, Fu Q and Gu Y, *Polymer* **175**:302–309 (2019).
55 Huang C-F, Chen W-H, Aimi J, Huang Y-S, Venkatesan S, Chiang Y-W *et al.*, *Polym Chem* **9**:5644–5654 (2018).
56 Goward GR, Schnell I, Brown SP, Spiess HW, Kim H-D and Ishida H, *Magn Reson Chem* **39**:S5–S17 (2001).
57 Kim H-D and Ishida H, *Chem Eur J* **106**:3271–3280 (2002).
58 Goward GR, Sebastiani D, Schnell I, Spiess HW, Kim H-D and Ishida H, *J Am Chem Soc* **125**:5792–5800 (2003).
59 Froimowicz P, Zhang K and Ishida H, *Chem Eur J* **22**:2691–2707 (2016).
60 Nagata Y and Chujo Y, *Macromolecules* **41**:3488–3492 (2008).
61 Yin X, Guo F, Lalancette RA and Jäkle F, *Macromolecules* **49**:537–546 (2016).
62 Younis O, Khamies A, Yang X and Aly KI, *Polym Adv Technol* **35**:e6521 (2024).

